(Received 25 July 2025, Accepted 11 September 2025, Scheduled 21 September 2025)

Robust and Flexible Synthesis of Equi-Ripple Multiband Filtering Functions in the Pole-Zero Form

Sai Peng[1], Jiyuan Fan[1], Ping Zhao[2,*], Nan Shen[3], Jinzhu Zhou[2], and Qingqiang Wu[3]

[1]*National Key Laboratory of Radar Detection and Sensing, Xidian University, Xi'an 710071, China*
[2]*State Key Laboratory of Electromechanical Integrated Manufacturing of High-Performance Electronic Equipments Xidian University, Xi'an 710000, China*
[3]*ZTE Corporation, Shenzhen 518057, China*

ABSTRACT: This paper presents a numerical iterative approach to synthesizing multiband filtering functions that can realize equi-ripple in-band responses and enforce the same return loss (RL) level across all passbands. By iteratively updating the reflection zeros (RZs) and some additional transmission zeros (TZs), the multiband filtering function can be constructed to give an equi-ripple characteristic and ensure the same RL levels in all passbands. The advantages of the proposed method include that equal RL level in all passbands can be enforced, and the numerical stability is improved over existing methods. The proposed method can be used to synthesize symmetric or asymmetric multiband filter (MBF) responses with an arbitrary number of passbands. Two synthesis examples are provided. The first example is a tri-band filter (TBF) with an RL level of 23 dB. Its passband frequency ranges are $\{(-1,-0.7),\ (-0.15,0.15),\ (0.7,1)\}$ rad/s, in the normalized frequency domain, and the numbers of poles in the three passbands are 5, 4, and 5, respectively. In the second example, a dual-band waveguide filter (DBF) with four poles in each passband is synthesized and designed. The frequency ranges of the two passbands are $\{(11.8,11.95),\ (12.085,12.2)\}$ GHz. Both simulated and measured RL levels of the filter are 22 dB. The measured insertion loss is 0.73 dB in the lower passband and 0.75 dB in the upper passband. The simulated and measured results are in excellent agreement with the theoretical response, thus verifying the proposed synthesis method.

1. INTRODUCTION

With the rapid advancement of wireless communication technologies, the integration of multiple applications into a single system has become a prevailing trend. If a single-band filter is used to serve each individual channel, the resulting radio frequency (RF) front-end becomes bulky and inefficient. In contrast, multiband filters (MBFs) can process signals across multiple non-contiguous frequency bands simultaneously, which makes a significant contribution to system integration and compactness. Therefore, flexible and effective synthesis approaches for MBFs are desired. Coupling matrix model is often used for designing high-performance MBFs. Coupling matrix must be synthesized in a target topology suitable for physical realization. Meanwhile, its frequency-domain characteristics should meet the design specifications [1–3]. Various methods for solving multiband filtering functions have been proposed to synthesize the target MBF coupling matrix.

The first method for synthesizing multiband filtering functions is frequency mapping method [4–8], which converts a single-band lowpass prototype filtering function into a multiband filtering function. Cameron et al. first used frequency mapping method to synthesize symmetric dual-band filters (DBF) [4]. However, since all the passbands originate from the same lowpass prototype by the frequency mapping, the number of reflection zeros (RZs) in each passband cannot be independently controlled. To achieve better flexibility, Chen et al. convert multiple lowpass prototype filtering functions into a multiband filtering function. This approach can flexibly realize different orders, bandwidths, or RL levels in different passbands [8–9]. However, this method cannot guarantee exact equi-ripple characteristics in passbands. The optimization method can also be used to synthesize multiband filtering functions, but it does not always converge to the optimal solution [10–12].

Another category of methods is numerical iterative technique [13–17]. The advantages of this type of method are that the frequency range, and the order of each passband can be independently controlled, while the response of each passband exhibits an exact equi-ripple characteristic. However, the return loss (RL) level of each passband cannot be arbitrarily specified [13]. To address this issue, Zhao and Wu [14] and Ren et al. [15] introduced an additional transmission zero (TZ) in the DBF to realize prescribed RL levels based on an improved Remez-like algorithm. However, the additional TZ may appear in one of the passbands. Recently, Zhao et al. introduced more redundant TZs and controlled them by adjusting extra parameters to make the multiband filter synthesis more robust [16]. All the above methods are based on variants of the Remez algorithm, which rely on interpolating in-band extrema. When the order of MBF is high, the numerical stability of these algorithms becomes poor due to the involvement of the Vandermonde matrix in interpolation equations. There is another iterative method that expresses multiband filtering functions in

* Corresponding author: Ping Zhao (aoing56@gmail.com).

the form of a pole-zero product [17], which can enhance the numerical stability of MBF synthesis. However, this method cannot flexibly control the RL level in each passband, which often results in unrealistic RL levels.

This paper proposes a novel numerical iterative method that introduces a set of additional TZs to the pole-zero form of multiband filtering function. The proposed method iteratively updates RZs and additional TZs until the multiband filtering function exhibits an equi-ripple characteristic in each passband, and all passbands have the same RL level. Compared to existing methods, this approach not only enables control over RL levels of all passbands but also merits better numerical stability when synthesizing high-order multiband filters. The rest of this paper is arranged as follows. Sections 2 describes the synthesis process of multiband filtering functions. Section 3 provides two synthesis examples to verify the effectiveness of the proposed method. Section 4 compares the proposed method with existing approaches. Finally, the conclusion is drawn.

2. SYNTHESIS METHOD

2.1. Filtering Function and Scattering Characteristics

The synthesis of an MBF begins with constructing a filtering function $C(\omega)$ that realizes equi-ripple responses and the same RL level in all passbands. Similar to a single-band filter, a multiband filtering function is expressed as the ratio of two polynomials:

$$C(\omega) = \frac{F(\omega)}{P(\omega)} \tag{1}$$

where ω is the normalized lowpass angular frequency, and $F(\omega)$ and $P(\omega)$ are monic polynomials. The order of $F(\omega)$ is N, where N is the degree of the filter. The roots of $F(\omega)$ are RZs of the filter. The order of $P(\omega)$ is *nz*, which is the number of finite-position TZs. The roots of $P(\omega)$ are the TZs of the filter.

With filtering function $C(\omega)$, S-parameter rational functions can be constructed. Assuming $nz < N$, S-parameters can be expressed as:

$$S_{11}(s) = \frac{F(s)}{E(s)}, \quad S_{21}(s) = \frac{P(s)}{\varepsilon E(s)} \tag{2}$$

where $s = j\omega$ is the normalized complex frequency, and j is the imaginary unit. $F(s)$ and $P(s)$ are polynomials in s which are converted from $F(\omega)$ and $P(\omega)$, respectively. ε is a real constant related to the RL level of the filter, and its value can be obtained by

$$\varepsilon = \frac{1}{\sqrt{10^{RL/10}-1}} \left| \frac{P(\omega)}{F(\omega)} \right| \Bigg|_{\omega=\omega_1} \tag{3}$$

where ω_1 is one of the band edge frequencies. $E(s)$ is a Hurwitz polynomial, which means that all its roots are in the left-half complex plane. According to the power conservation condition, $E(s)$ should satisfy the following equation

$$E(s)E^*(s) = F(s)F^*(s) + \frac{1}{\varepsilon^2}P(s)P^*(s) \tag{4}$$

where superscript * denotes the para-conjugation [18].

MBF synthesis first solves an appropriate filtering function $C(\omega)$. Then, polynomials $F(s)$, $P(s)$, $E(s)$, and ε are constructed. Finally, the coupling matrix of the filter can be synthesized from S-parameter rational functions.

2.2. Iterative Construction of the Filtering Function

The rational filtering function $C(\omega)$ can be written in a pole-zero form as:

$$C(\omega) = \frac{F(\omega)}{P(\omega)} = \frac{\prod_{j=1}^{N}(\omega - r_j)}{\prod_{m=1}^{nz-(M-1)}(\omega - z_m)\prod_{t=1}^{M-1}(\omega - z_t)} \tag{5}$$

where r_j, $j = 1, \ldots, N$ are the RZs, and z_m, $m = 1, \ldots, nz-(M-1)$ are the prescribed TZs, where M is the number of passbands. z_t, $t = 1, \ldots, M-1$ are additional TZs. The values of z_t will be determined in the iterative synthesis process for the independent control of RL levels in each passband. In this work, these additional TZs are introduced to make the RL levels of all passbands equal. There is one additional TZ in each inner stopband. Since there are M passbands, $(M-1)$ additional TZs are introduced. The core idea of the multiband filtering function synthesis is to iteratively update r_j and z_t until $C(\omega)$ realizes equi-ripple filter responses in each passband, and RL levels of all passbands are equal.

In the beginning, a set of initial r_j is given, whose values can be set evenly distributed in each passband. The initial values of z_t can be chosen at the center of each internal stopband. It is worth noting that we can also select other values as the initial RZs and additional TZs. The convergence of the proposed method is insensitive to the choice of initial RZs and additional TZs.

After obtaining the initial RZs and TZs, we can construct the initial filtering function $C(\omega)$ and determine the positions where $C(\omega)$ reaches its in-band extrema by numerical methods. Assume that the frequency points at which $C(\omega)$ reaches the extrema values within the i-th passband are $\omega_{i_1}, \ldots, \omega_{i_{K-1}}$, where K is the number of RZs in this passband. Let ω_{i_0} and ω_{i_K} denote the lower and upper edge frequencies of the i-th passband, respectively. Then, $\omega_{i_0} < \omega_{i_1} < \ldots < \omega_{i_k} < \ldots < \omega_{i_{K-1}} < \omega_{i_K}$. Each RZ in the passband should be located between two adjacent extrema, that is, $\omega_{i_{k-1}} < r_{i_k} < \omega_{i_k}$. In the beginning, the absolute values of the in-band extrema of $C(\omega)$ based on the initial r_j and z_t are usually not equal. Therefore, it is necessary to update r_j and z_t of $C(\omega)$ to make them approaching their optimal positions such that each passband presents equi-ripple characteristics, and RL levels of all passbands are equal.

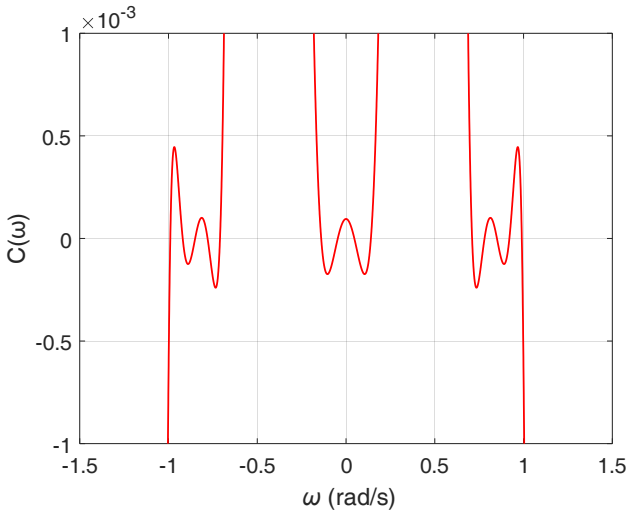

FIGURE 1. The initial tri-band filtering function $C(\omega)$.

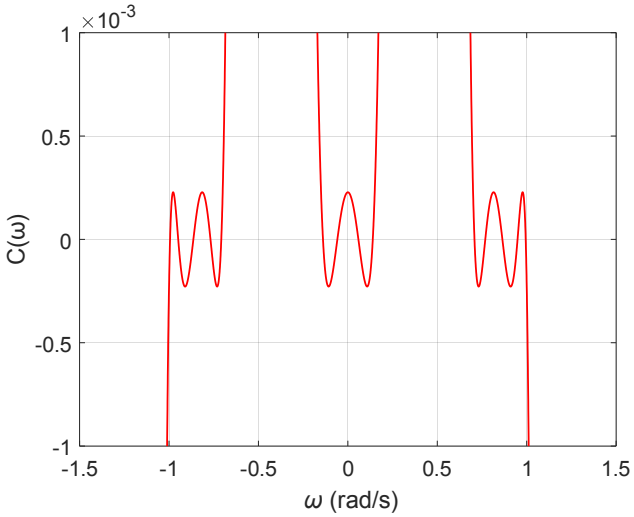

FIGURE 2. The final tri-band filtering function $C(\omega)$.

The position of r_j is updated first. Let $C_0(\omega)$ be the filtering function before updating r_j and $C_1(\omega)$ be

$$C_1(\omega) = \left(\omega - r'_{i_k}\right) * \frac{\prod_{j=1, j\neq i_k}^{N} (\omega - r_j)}{\prod_{m=1}^{nz-(M-1)} (\omega - z_m) \prod_{t=1}^{M-1} (\omega - z_t)} \tag{6}$$

where r'_{i_k} is the updated value of r_{i_k}, so that absolute values of the function $C_1(\omega)$ at the two adjacent extreme points ω_{i_k} and $\omega_{i_{k+1}}$ are equal, and their signs are the opposite, that is

$$C_1(\omega_{i_k}) = -C_1(\omega_{i_{k+1}}). \tag{7}$$

Substituting (6) into (7) yields:

$$\frac{(\omega_{i_k} - r'_{i_k})}{(\omega_{i_k} - r_{i_k})} C_0(\omega_{i_k}) = -\frac{(\omega_{i_{k+1}} - r'_{i_k})}{(\omega_{i_{k+1}} - r_{i_k})} C_0(\omega_{i_{k+1}}). \tag{8}$$

Through further manipulations, the explicit updating expression of r'_{i_k} can be obtained using (9).

$$r'_{i_k} = \frac{r_{i_k}\left[\omega_{i_k} C_0(\omega_{i_k}) + \omega_{i_{k+1}} C_0(\omega_{i_{k+1}})\right] - \omega_{i_k}\omega_{i_{k+1}}\left[C_0(\omega_{i_k}) + C_0(\omega_{i_{k+1}})\right]}{r_{i_k}\left[C_0(\omega_{i_k}) + C_0(\omega_{i_{k+1}})\right] - \left[\omega_{i_{k+1}} C_0(\omega_{i_k}) + \omega_{i_k} C_0(\omega_{i_{k+1}})\right]} \tag{9}$$

RZs $r_1, r_2, \ldots, r_N$ are updated one by one by (9). After all the RZs are updated, the additional TZs are updated one by one. Let $C_2(\omega)$ be the filtering function after updating z_l, and its expression is

$$C_2(\omega) = \frac{1}{(\omega - z'_l)} * \frac{\prod_{j=1}^{N} (\omega - r_j)}{\prod_{m=1}^{nz-(M-1)} (\omega - z_m) \prod_{t=1, t\neq l}^{M-1} (\omega - z_t)} \tag{10}$$

where z'_l represents the updated value of $z_l (l = 1, \ldots, M-1)$. Its value is determined such that the absolute values of $C_2(\omega)$ at the upper edge frequency of the i-th passband and the lower edge frequency of the $(i+1)$-th passband are equal, that is

$$C_2(\omega_{i_H}) = \pm C_2(\omega_{i+1_L}). \tag{11}$$

Note that when the number of TZs between the two adjacent passbands is even, the signs of $C_2(\omega_{i_H})$ and $C_2(\omega_{i+1_L})$ are the same. Otherwise, their signs are opposite. Substituting (10) into (11) yields the following equation:

$$\frac{\omega_{i_H} - z_l}{\omega_{i_H} - z'_l} C_0(\omega_{i_H}) = \pm \frac{\omega_{i+1_L} - z_l}{\omega_{i+1_L} - z'_l} C_0(\omega_{i+1_L}) \tag{12}$$

After some manipulations, the explicit updating equation of z'_t can be obtained using (13).

One iteration is completed after updating all the RZs r_j and additional TZs z_t once. Then, multiband filtering function $C(\omega)$ is updated. A numerical method can be applied to the updated filtering function $C(\omega)$ to identify the frequencies ω_{i_k} where $C(\omega)$ reaches in-band extrema. Then, the iteration repeats to update r_j and z_t until convergence. After convergence, the filtering function realizes equi-ripple filter responses in each passband and same RL levels of all passbands. The target rational expression of the S-parameters for the MBF can be constructed according to the procedure described in Subsection 2.1. Then, the coupling matrix of the filter can be synthesized following well-established techniques to guide the physical structure design of the MBF.

TABLE 1. The positions of RZs and additional TZs after each iteration.

Iteration	0th	1st	2nd	3rd	4th	5th	6th	7th	8th	9th	10th
r_1	−0.9500	−0.9960	−0.9925	−0.9943	−0.9940	−0.9942	−0.9942	−0.9942	−0.9942	−0.9943	−0.9943
r_2	−0.9000	−0.9153	−0.9503	−0.9453	−0.9481	−0.9479	−0.9484	−0.9484	−0.9485	−0.9486	−0.9486
r_3	−0.8500	−0.8520	−0.8556	−0.8617	−0.8618	−0.8631	−0.8633	−0.8636	−0.8637	−0.8638	−0.8639
r_4	−0.8000	−0.7883	−0.7605	−0.7665	−0.7670	−0.7674	−0.7678	−0.7680	−0.7681	−0.7681	−0.7682
r_5	−0.7500	−0.7051	−0.7088	−0.7072	−0.7077	−0.7077	−0.7078	−0.7078	−0.7078	−0.7078	−0.7078
r_6	−0.0900	−0.1422	−0.1384	−0.1397	−0.1390	−0.1392	−0.1391	−0.1392	−0.1392	−0.1392	−0.1392
r_7	−0.0300	−0.0398	−0.0674	−0.0555	−0.0601	−0.0582	−0.0589	−0.0587	−0.0588	−0.0588	−0.0588
r_8	0.0300	0.0398	0.0674	0.0555	0.0601	0.0582	0.0589	0.0587	0.0588	0.0588	0.0588
r_9	0.0900	0.1422	0.1384	0.1397	0.1390	0.1392	0.1391	0.1392	0.1392	0.1392	0.1392
r_{10}	0.7500	0.7051	0.7088	0.7072	0.7077	0.7077	0.7078	0.7078	0.7078	0.7078	0.7078
r_{11}	0.8000	0.7883	0.7605	0.7665	0.7670	0.7674	0.7678	0.7680	0.7681	0.7681	0.7682
r_{12}	0.8500	0.8520	0.8556	0.8617	0.8618	0.8631	0.8633	0.8636	0.8637	0.8638	0.8639
r_{13}	0.9000	0.9153	0.9503	0.9453	0.9481	0.9479	0.9484	0.9484	0.9485	0.9486	0.9486
r_{14}	0.9500	0.9960	0.9925	0.9943	0.9940	0.9942	0.9942	0.9942	0.9942	0.9943	0.9943
z_1	−0.4250	−0.3285	−0.3766	−0.3590	−0.3683	−0.3620	−0.3594	−0.3585	−0.3570	−0.3567	−0.3562
z_2	0.4250	0.3285	0.3766	0.3590	0.3683	0.3620	0.3594	0.3585	0.3570	0.3567	0.3562

3. SYNTHESIS AND DESIGN EXAMPLES

3.1. Synthesis of a Symmetric Tri-Band Filter

The first example is a tri-band filter (TBF) whose passband frequency ranges in the normalized frequency domain are $\{(-1,-0.7),(-0.15,0.15),(0.7,1)\}$ rad/s. The numbers of RZs in the three passbands are five, four, and five, respectively. That is, $N_1 = N_3 = 5$ and $N_2 = 4$, and the total degree of the TBF is $N = 14$. The desired in-band RL level is 23 dB for all passbands. The prescribed TZs are located at $\{-1.185,-0.565,0.565,1.185\}$ rad/s. Since there are three passbands, two additional TZs z_1 and z_2 are introduced to control RL levels of the passbands.

In the beginning, the initial RZs are chosen evenly distributed within each passband, and the initial additional TZs are chosen at the center of each internal stopband. The initial TZs include prescribed TZs and additional TZs. Based on the initial RZs and TZs, a filter function $C(\omega)$ can be obtained, whose response exhibits non-equi-ripple characteristics within each passband, as shown in Fig. 1.

By the iterative technique in Section 3, RZs and additional TZs of the tri-band filtering function are iteratively updated. The values of r_j and z_t obtained during the iteration process are listed in Table 1. It is seen that RZs and additional TZs become stable after a few iterations. After convergence, the coefficients of polynomials $F(\omega)$ and $P(\omega)$ can be derived based on RZs and TZs, as shown in Table 2, and the final filtering function $C(\omega)$ is plotted in Fig. 2. We can see that $C(\omega)$ realizes equi-ripple characteristics in each passband and has the same amplitude in all passbands. Then, the filtering function is used to construct S-parameter polynomials, as described in Section 2. Fig. 3 shows the scattering characteristics of the TBF, whose response is equi-ripple in each passband, and RL levels of all passbands are equal.

$$z_l' = \frac{z_l\left[\omega_{i+1_L}C_0\left(\omega_{i_H}\right)+\omega_{i_H}C_0\left(\omega_{i+1_L}\right)\right]-\omega_{i_H}\omega_{i+1_L}\left[C_0\left(\omega_{i_H}\right)+C_0\left(\omega_{i+1_L}\right)\right]}{z_l\left[C_0\left(\omega_{i_H}\right)+C_0\left(\omega_{i+1_L}\right)\right]-\left[\omega_{i+1_L}C_0\left(\omega_{i+1_L}\right)+\omega_{i_H}C_0\left(\omega_{i_H}\right)\right]} \tag{13}$$

After the S-parameter polynomials are obtained, they are converted into Y-parameter polynomials. Then, a transversal coupling matrix of the TBF is synthesized [1, 18]. The transversal coupling matrix can be converted into the target form corresponding to the coupling topology in Fig. 4 through a series of similarity transformations [19]. The final coupling coefficients are labeled in the coupling diagram in Fig. 4.

3.2. Design of an Asymmetric Dual-band Filter

In the second example, an H-plane WR-75 waveguide filter is designed based on the proposed synthesis method. The frequency ranges of the two passbands are $11.8 \sim 11.95$ GHz and $12.085 \sim 12.2$ GHz, respectively. The prescribed TZs are at 11.76 GHz, 12.049 GHz, and 12.235 GHz. The physical frequency is first transformed into the normalized frequency do-

TABLE 2. Coefficients of S-parameter polynomials.

$\omega^i, i =$	$F(\omega)$	$P(\omega)$	$E(\omega)$
0	0	-0.0577	-0.0002
1	0	0	$-0.0026i$
2	0.0046	0.6770	0.0212
3	0	0	0.1081i
4	-0.2287	-1.8738	-0.4179
5	0	0	$-0.8958i$
6	1.4950	1	2.3328
7	0		2.9993i
8	-4.0771		-5.7813
9	0		$-4.7879i$
10	5.5552		7.1481
11	0		3.6317i
12	-3.7489		-4.3023
13	0		$-1.0521i$
14	1		1
$\varepsilon = 311.0026$			

main by the bandpass-to-lowpass mapping

$$\omega = \frac{f_0}{BW}\left(\frac{f}{f_0} - \frac{f_0}{f}\right) \tag{14}$$

where $f_0 = 11.998\,\text{GHz}$ and $BW = 0.4\,\text{GHz}$ are the center frequency and bandwidth of the whole DBF, respectively. The two passbands in the normalized frequency domain are $[-1, -0.2422]$ rad/s and $[0.4318,\ 1]$ rad/s, respectively. The prescribed TZs are located at $\{-1.2037, 0.2528, 1.1719\}$ rad/s. Each of the passbands has four in-band RZs. The target RL level is 22 dB for both passbands.

The iterative technique in Section 3 is used to synthesize the asymmetric dual-band filtering function. After the iteration converges, the final RZs (r_j) are: -0.9825, -0.8289, -0.5292, -0.2772, 0.4504, 0.6107, 0.8507, 0.9846, and the additional TZ is $z_t = 0.1236$.

Based on converged RZs and TZs, coefficients of $F(\omega)$ and $P(\omega)$ can be obtained. Then, following the procedure in Section 2, the S-parameter rational functions are constructed. After the S-parameter rational functions are converted into Y-parameters, the transversal coupling matrix of the DBF is synthesized [1, 18] from the partial fraction expansions of Y-parameters. After a series of matrix transformations [19–23], the transversal coupling matrix is converted into a cascaded-quartet coupling topology, as shown in Fig. 5. In this example, the first quartet realizes the TZs $\{-1.2037, 1.1719\}$ rad/s, and the second quartet realizes the TZs $\{\ 0.1236,\ 0.2528\}$ rad/s. Note that the main-line couplings M_{34} and M_{78} are two frequency-dependent couplings [20–23], which are introduced to annihilate diagonal cross-couplings that are inconvenient for physical realization.

The final coupling matrix and capacitance matrix of the DBF are shown in Tables 3 and 4, respectively. An H-plane WR-75 waveguide filter was designed based on these two matrices. The WR-75 waveguide has a size of $a = 19.05\,\text{mm}$ and $b = 9.525\,\text{mm}$. The electromagnetic (EM) model of the filter is presented in Fig. 6, with its geometrical dimensions marked in the layout. The small cylinders in Fig. 6(a) represent M2.5 tuning screws, which are provisioned on the top cover of the filter. The penetration depth of all tuning screws is 1.5 mm. All the resonators are realized as TE_{101} mode rectangular waveguide cavities. Inductive irises are used to realize positive couplings. Frequency-dependent couplings M_{34} and M_{78} are implemented by partial-height metal posts whose positions are offset from the centers. The filter's EM model is fine-tuned with the aid of the model-based vector fitting technique [24, 25]. The simulated filter response and synthesized coupling matrix response are compared in Fig. 7. A decent agreement between simulated and theoretical responses is achieved, verifying the proposed synthesis method.

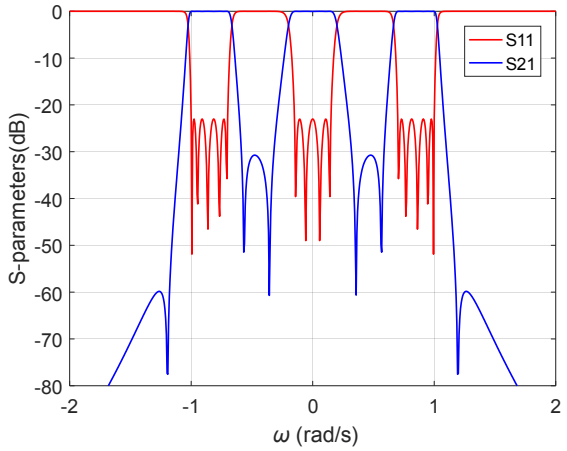

FIGURE 3. TBF response synthesized with the proposed approach.

The DBF is fabricated with aluminum and silver plated. Fig. 8 shows a photograph of the rectangular waveguide filter. In Fig. 9, measured S-parameters of the DBF are plotted with solid lines, and the synthesized coupling matrix response is shown by dashed lines. The measured response shows good agreement with the synthesized response, validating the synthesis results and confirming the feasibility of the physical realization.

4. COMPARISON WITH EXISTING METHOD

This section demonstrates the improvement of the proposed method over the existing method through two examples. The first example has the following specifications:

The normalized passband frequency ranges (rad/s): $\{(-1 - 0.4), (0.6\ 1)\}$.

Orders of the channel: $\{4, 4\}$.

Prescribed TZs (rad/s): $\{-1.3, 0.18, 1.46\}$.

RL in each passband (dB): $\{22, 22\}$.

As shown in Fig. 10, the method in [17] may result in significantly different RL levels between the two passbands. One of the passbands has very high RL level while the other has a relatively low RL level. To address this issue, an additional TZ

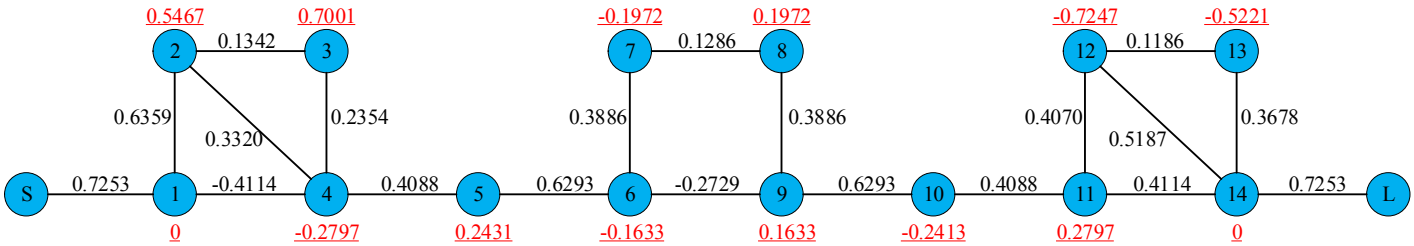

FIGURE 4. The target coupling topology of the TBF. Hollow circles with numbers inside are resonators. The numbers without underscores are off-diagonal entries (IO and mutual couplings), and the numbers with underscores are diagonal entries (self-couplings).

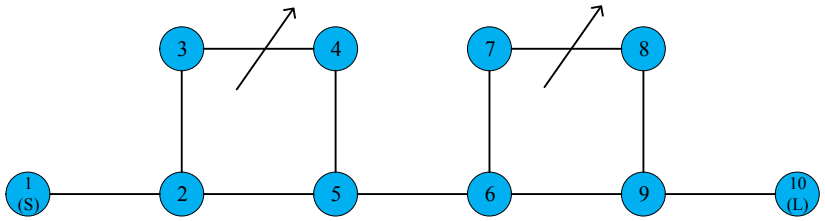

FIGURE 5. The target coupling topology of the DBF. Hollow circles with numbers inside are resonatoes. Solid lines are couplings. Solid line segments with arrows denote frequency-dependent couplings.

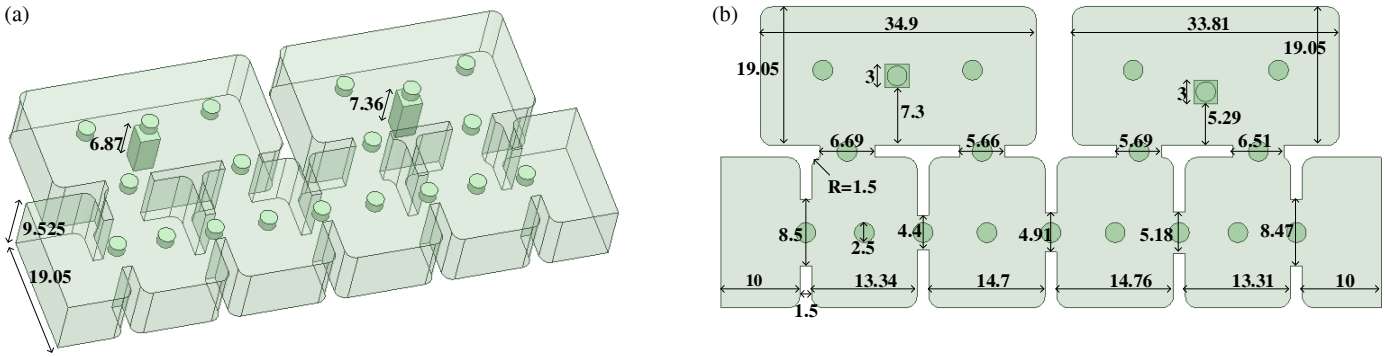

FIGURE 6. EM model of filter in the second example. The geometrical dimensions are with unit mm. The small cylinders on the top are M2.5 tuning screws. (a) Perspective view. (b) Top view.

TABLE 3. Coupling matrix M corresponding to Figure 5.

	1(S)	2	3	4	5	6	7	8	9	10(L)
1(S)	0	0.8669	0	0	0	0	0	0	0	0
2	0.8669	0.0454	0.7236	0	0.3711	0	0	0	0	0
3	0	0.7236	−0.0817	−0.7900	0	0	0	0	0	0
4	0	0	−0.7900	0.0027	0.5088	0	0	0	0	0
5	0	0.3711	0	0.5088	−0.0628	0.5076	0	0	0	0
6	0	0	0	0	0.5076	0.1222	0.4199	0	0.6233	0
7	0	0	0	0	0	0.4199	−0.2618	−0.0127	0	0
8	0	0	0	0	0	0	−0.0217	−0.1568	0.5197	0
9	0	0	0	0	0	0.6233	0	0.5197	0.0454	0.8669
10(L)	0	0	0	0	0	0	0	0	0.8669	0

TABLE 4. Capacitance matrix C corresponding to Figure 5.

	1(S)	2	3	4	5	6	7	8	9	10(L)
1(S)	0	0	0	0	0	0	0	0	0	0
2	0	1	0	0	0	0	0	0	0	0
3	0	0	1	0.0430	0	0	0	0	0	0
4	0	0	0.0430	1	0	0	0	0	0	0
5	0	0	0	0	1	0	0	0	0	0
6	0	0	0	0	0	1	0	0	0	0
7	0	0	0	0	0	0	1	0.1171	0	0
8	0	0	0	0	0	0	0.1171	1	0	0
9	0	0	0	0	0	0	0	0	1	0
10(L)	0	0	0	0	0	0	0	0	0	0

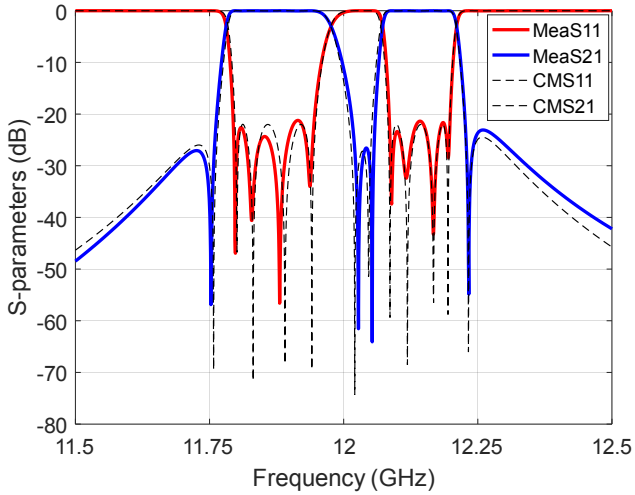

FIGURE 7. DBF response synthesized and designed by the proposed approach. Solid lines: EM simulation results. Dashed lines: responses of the synthesized coupling matrix.

FIGURE 8. Photograph of the fabricated dual-band rectangular waveguide filter.

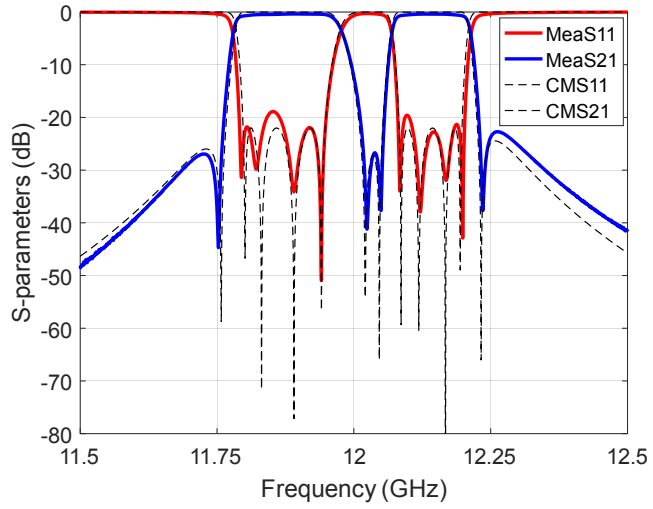

FIGURE 9. Comparison between measurement results and S-parameters of the synthesized coupling matrix. Solid lines: measured results. Dashed lines: responses of the synthesized coupling matrix.

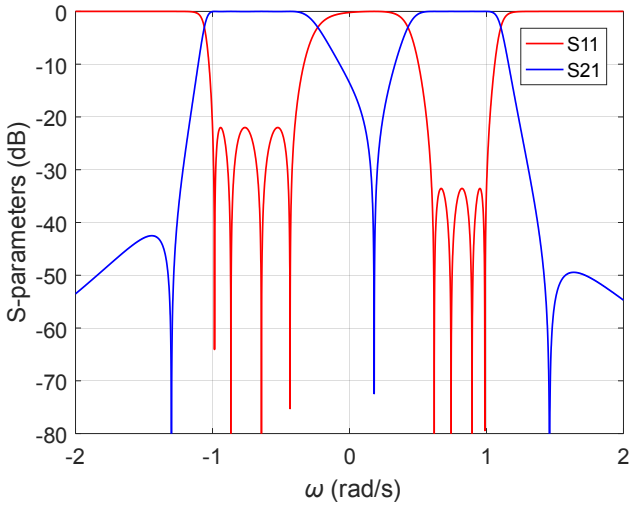

FIGURE 10. DBF responses synthesized by the existing method [17].

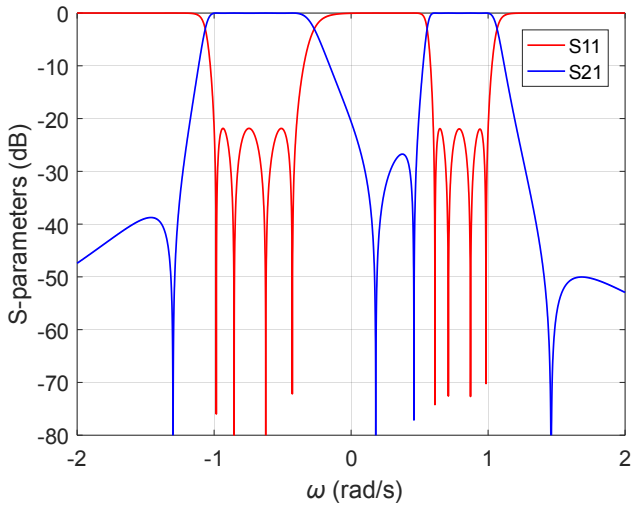

FIGURE 11. DBF responses synthesized by the proposed approach.

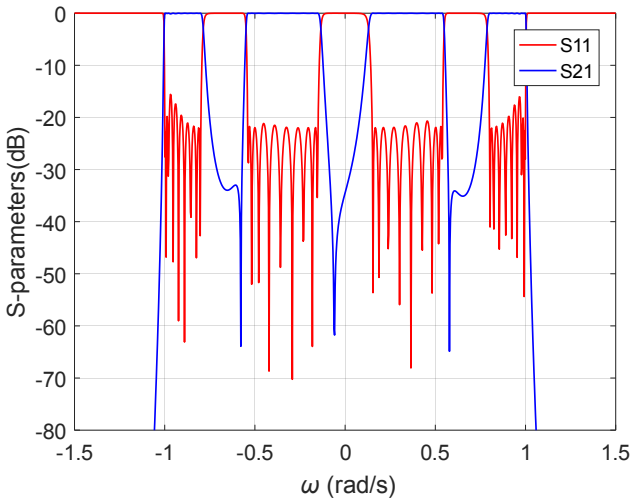

FIGURE 12. Quad-band filter synthesized by the existing method.

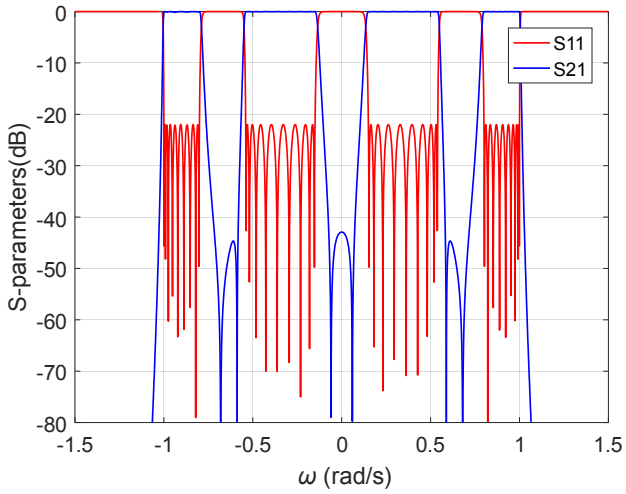

FIGURE 13. Quad-band filter synthesized by the proposed approach.

is introduced in this work, enabling the same RL level across all passbands, as demonstrated in Fig. 11.

The second example has the following specifications:

The normalized passband frequency ranges (rad/s): $\{(-1\ -0.8), (-0.54\ -0.15), (-0.15\ 0.54), (0.8\ 1)\}$.

Orders of the channel: $\{9, 9, 9, 9\}$.

Prescribed TZs (rad/s): $\{-1.3074, -0.5883, -0.0600, 0.5883, 1.3074\}$.

Additional TZs (rad/s): $\{-0.6804, 0.0600, 0.6804\}$.

RL in each passband (dB): $\{22, 22, 22, 22\}$.

The numerical stability of Remez-like algorithms introduced in [14–16] deteriorates when this high-order filter is synthesized, due to the involvement of the Vandermonde matrix in the interpolation equation. Significant numerical errors exist in the iterative calculation of in-band extreme points, leading to non-equiripple filter responses. As shown in Fig. 12, S-parameters of the first and fourth channels deviate from equiripple characteristics. Empirically, existing Remez-like algorithms can accurately synthesize multiband filters up to a degree of 30. In contrast, the proposed method can synthesize higher-order multiband filters, as shown by synthesis results of the 36th-order quad-band filter in Fig. 13.

5. CONCLUSION

This article introduces an iterative synthesis method for synthesizing multiband filtering functions that exhibit equi-ripple responses within all passbands while maintaining the same RL levels in each band. Additional TZs are determined during the filtering function synthesis process to ensure that the RL levels in all passbands are equal. The proposed method also exhibits better numerical stability when synthesizing high-order multiband filters. The approach allows the synthesis of both symmetric and asymmetric multiband filter responses, offering significant flexibility in meeting diverse design requirements. Two filter synthesis examples are provided to validate the feasibility of the proposed method. Moreover, the advantages of the proposed method over existing methods are demonstrated through synthesis examples.

ACKNOWLEDGEMENT

This work was supported in part by the National Natural Science Foundation of China under Grant 62471366 and Grant 52175247, in part by the Natural Science Basic Research Program of Shaanxi under Grant 2023-JC-JQ-43, and in part by the Key Core Technology Research and Development Project of Key Industrial Chains in Xi'an under Grant 23LLRH0080.

REFERENCES

[1] Cameron, R. J., "Advanced coupling matrix synthesis techniques for microwave filters," *IEEE Transactions on Microwave Theory and Techniques*, Vol. 51, No. 1, 1–10, 2003.

[2] Cameron, R. J., "Advanced synthesis techniques for microwave filters," *ZTE Communications*, Vol. 9, No. 2, 27, 2011.

[3] Djianga, A. N., C. Mbinack, G. A. Eyebe, P. Zhao, and J. S. A. E. Fouda, "Design and simultaneous analytical optimization of mi-

crowave filters with superimposed rectangular cavities for radar applications," *AEU — International Journal of Electronics and Communications*, Vol. 188, 155572, 2025.

[4] Cameron, R. J., M. Yu, and Y. Wang, "Direct-coupled microwave filters with single and dual stopbands," *IEEE Transactions on Microwave Theory and Techniques*, Vol. 53, No. 11, 3288–3297, 2005.

[5] Macchiarella, G. and S. Tamiazzo, "Design techniques for dual-passband filters," *IEEE Transactions on Microwave Theory and Techniques*, Vol. 53, No. 11, 3265–3271, 2005.

[6] Lee, J. and K. Sarabandi, "Design of triple-passband microwave filters using frequency transformations," *IEEE Transactions on Microwave Theory and Techniques*, Vol. 56, No. 1, 187–193, 2008.

[7] Di, H., B. Wu, X. Lai, and C.-H. Liang, "Synthesis of cross-coupled triple-passband filters based on frequency transformation," *IEEE Microwave and Wireless Components Letters*, Vol. 20, No. 8, 432–434, 2010.

[8] Chen, X., L. Zhang, C. Xu, Z. Zheng, and X. Jiang, "Dual-band filter synthesis based on two low-pass prototypes," *IEEE Microwave and Wireless Components Letters*, Vol. 27, No. 10, 903–905, 2017.

[9] Chen, X., "Synthesis of multi-band filters based on multi-prototype transformation," *IET Microwaves, Antennas & Propagation*, Vol. 15, No. 2, 103–114, 2021.

[10] Bila, S., R. J. Cameron, P. Lenoir, V. Lunot, and F. Seyfert, "Chebyshev synthesis for multi-band microwave filters," in *2006 IEEE MTT-S International Microwave Symposium Digest*, 1221–1224, San Francisco, CA, USA, 2006.

[11] Lunot, V., S. Bila, and F. Seyfert, "Optimal synthesis for multi-band microwave filters," in *2007 IEEE/MTT-S International Microwave Symposium*, 115–118, Honolulu, HI, USA, 2007.

[12] Lunot, V., F. Seyfert, S. Bila, and A. Nasser, "Certified computation of optimal multiband filtering functions," *IEEE Transactions on Microwave Theory and Techniques*, Vol. 56, No. 1, 105–112, 2008.

[13] Macchiarella, G., ""equi-ripple" synthesis of multiband prototype filters using a remez-like algorithm," *IEEE Microwave and Wireless Components Letters*, Vol. 23, No. 5, 231–233, 2013.

[14] Zhao, P. and K. Wu, "Iterative synthesis of equi-ripple dual-band filtering functions with one additional transmission zero," in *2019 IEEE MTT-S International Microwave Symposium (IMS)*, 1351–1354, Boston, MA, USA, 2019.

[15] Ren, X., Y. He, and L. Sun, "Advanced iterative synthesis of equiripple dual-band filters with fully prescribed performance," *IEEE Microwave and Wireless Technology Letters*, Vol. 33, No. 9, 1255–1257, 2023.

[16] Zhao, X., Y. He, and L. Sun, "Robust synthesis of multiband filters based on transmission zero redundancy method," *IEEE Microwave and Wireless Technology Letters*, Vol. 35, No. 8, 1126–1129, 2025.

[17] Zhang, Y., K. A. Zaki, J. A. Ruiz-Cruz, and A. E. Atia, "Analytical synthesis of generalized multi-band microwave filters," in *2007 IEEE/MTT-S International Microwave Symposium*, 1273–1276, Honolulu, HI, USA, 2007.

[18] Cameron, R. J., C. M. Kudsia, and R. R. Mansour, *Microwave Filters for Communication Systems: Fundamentals, Design, and Applications*, John Wiley & Sons, 2018.

[19] Tamiazzo, S. and G. Macchiarella, "An analytical technique for the synthesis of cascaded N-tuplets cross-coupled resonators microwave filters using matrix rotations," *IEEE Transactions on Microwave Theory and Techniques*, Vol. 53, No. 5, 1693–1698, 2005.

[20] Zhao, P. and K. Wu, "Cascading fundamental building blocks with frequency-dependent couplings in microwave filters," *IEEE Transactions on Microwave Theory and Techniques*, Vol. 67, No. 4, 1432–1440, 2019.

[21] He, Y., G. Macchiarella, Z. Ma, and N. Yoshikawa, "Synthesis and design of quasi-canonical planar filters comprising cascaded frequency-variant blocks," *IEEE Transactions on Microwave Theory and Techniques*, Vol. 69, No. 1, 671–681, 2021.

[22] Zhao, P. and K. Wu, "Filters with linear frequency-dependent couplings: Matrix synthesis and applications," *IEEE Microwave Magazine*, Vol. 24, No. 9, 30–45, 2023.

[23] Xiong, Z., P. Zhao, J. Fan, Z. Wu, and H. Gong, "Mixed electric and magnetic coupling design based on coupling matrix extraction," *ZTE Communications*, Vol. 21, No. 4, 85, 2023.

[24] Zhao, P., "Phase de-embedding of narrowband coupled-resonator networks by vector fitting," *IEEE Transactions on Microwave Theory and Techniques*, Vol. 71, No. 4, 1439–1446, 2023.

[25] Zhao, P. and K.-L. Wu, "Model-based vector-fitting method for circuit model extraction of coupled-resonator diplexers," *IEEE Transactions on Microwave Theory and Techniques*, Vol. 64, No. 6, 1787–1797, 2016.